AIMS Materials Science, 9(3): 430–445.
DOI: 10.3934/matersci.2022025
Received: 17 January 2022
Revised: 27 March 2022
Accepted: 08 April 2022
Published: 31 May 2022

http://www.aimspress.com/journal/Materials

Research article

Hybrid agarose gel for bone substitutes

Rémi G. Tilkin[1,2,*], Ana P. F. Monteiro[1,2,*], Julien G. Mahy[1,3], Jérome Hurlet[2], Nicolas Régibeau[1,2], Christian Grandfils[2] and Stéphanie D. Lambert[1]

[1] Department of Chemical Engineering–Nanomaterials, Catalysis and Electrochemistry (NCE), University of Liège, Allée du Six Août 11, 4000 Liège, Belgium
[2] Centre Interfacultaire des Biomatériaux (CEIB), University of Liège, Allée du Six Août 11, 4000 Liège, Belgium
[3] Institute of Condensed Matter and Nanosciences (IMCN), Université catholique de Louvain, Place Louis Pasteur 1, 1348, Louvain-la-Neuve, Belgium

* **Correspondence:** Email: remitilkin@gmail.com, a.monteiro@uliege.be; Tel: +32498825292.

Abstract: Over the last decades, different materials have been investigated to overcome some flaws of bone substitutes. Even though various materials have been proposed for this conception, the in vivo assessments have still highlighted a lack of bioactivity and integration. In this context, this work focuses on the development of hybrid gel with surface properties specifically designed to promote bone regeneration by a sustained local delivery of active agents. We propose a new approach using modified-silica with high specific surface area and superior hydrophilicity dispersed in agarose hydrogel. In this optic, silica particles were dispersed in agarose solutions before the gelation of the composite upon cooling. The dispersion of the silica particles in the agarose gel was determined via scanning electronic microscopy. The degradation of the silica/agarose gels was also studied over a period of 12 weeks. Finally, the influence of the addition of silica on the permeability of the agarose gel was assessed via a diffusion test. The results showed that modified-silica particles exhibit a wide size distribution (500 nm and 10 µm) and can form clusters with higher size after their dispersion in agarose (up to 100 µm). The hybrid gel was stable over 12 weeks in aqueous solution. Moreover, no difference in permeability was noted between the hybrid gel and agarose hydrogel, allowing molecules up to 3 nm in diameter to diffuse freely within 1 mm thick agarose gels in less than 24 h. The present results indicate that hybrid agarose gel could represent an attractive matrix to disperse silica for scaffold applications.

Keywords: agarose; drug delivery; mesoporous materials; organosilane; silica gel

1. Introduction

Worldwide, over 4 million surgical operations involving bone grafting or bone graft substitutes are performed every year [1]. Bone represents the second most grafted organ after blood transfusion [2]. The importance of bone repair is expected to increase continuously in the next decades with the population aging (i.e. almost doubling of the population over 65 years in 2050) and the constant increase of need for healthcare worldwide [3].

Bone possesses the capacity of self-regeneration, allowing its repair without any scar [4,5]. However, in numerous cases, a bone substitute should be used in order to enhance tissue regeneration. If these approaches are successful in several clinical situations, they show important drawbacks like a limited lifetime, a lack of donors, or rejection of the bone grafts [6,7]. Moreover, in the case of synthetic substitutes, studies have recurrently shown a lack of cell differentiation, bone production, and bone integration [8,9].

In order to overcome these problems, the scientific community has explored new approaches in the field of tissue engineering. One promising strategy is the use of biodegradable scaffolds with surface specifically designed to promote bone regeneration by a sustained local delivery of active agents. Recently, silica gels have gained increasing interest in the tissue-engineering field, notably for the encapsulation and controlled release of different biomolecules [10–15]. These materials exhibits a large specific surface area, allowing the absorption of a large amount of biomolecules at the surface of the pores [16]. Additionally, the morphology of the pores can be tuned depending on the synthesis conditions (e.g. pH, solvent, processing conditions) in order to regulate the release process via different interactions between the guest molecules and the host pores [15,17,18]. The surface chemistry can also be modified to include functional groups presenting different charges or hydrophilic/hydrophobic properties to modulate the interactions between the pores and the proteins (i.e. electrostatic forces, hydrogen bonding, van der Waals forces, and covalent interactions). Moreover, silica is also very interesting from a biocompatible point of view being resorbable and non-toxic [16,19–21].

According to this approach, silica loaded with active macromolecules can be deposited at the surface of bone scaffold in order to improve bone repair process. Polymeric matrices have been proposed to disperse silica particles and facilitate the coating of silica beads on the surface of implant [22–25]. Various techniques, such as dip-coating or casting have been described to perform this physical coating in conditions preventing a denaturation of the active biomolecule [26–28].

In this optic, we propose in this work a hybrid hydrogel, prepared by dispersing silica particles in agarose gel, as a coating material for bone scaffolds. A matrix is necessary to enhance the deposition of silica particles at the surface of the scaffold. The agarose was selected due to its biocompatibility and thermo-gel reversible properties [29–31]. Another advantage of agarose gels is their porosity. Indeed, their pore size (i.e. 100 to 300 nm) is enough to allow the diffusion of the large biomolecules [32,33]. Moreover, their porosity can be tuned via the concentration and type of agarose, which in turn affect the biomolecule diffusion. Agarose has already been used as scaffold for bone regeneration but not combined with silica [34,35].

Specifically, our approach has used modified-silica containing ethylene diamine groups in order

to promote a better dispersion of silica in the agarose matrix. This modified silica may exhibit high specific surface area, superior hydrophilicity, and less aggregates forms in comparison to non-modified silica [36,37]. This work includes the preparation of the hybrid gels using agarose and this modified-silica, as well as a study of their morphology and dissolution. Moreover, the permeability of the hybrid gel is analyzed via the diffusion of polyethylene glycol markers.

2. Materials and methods

2.1. Materials

Tetraethyl orthosilicate (TEOS, $Si(OC_2H_5)_4$), ammonium hydroxide solution NH_3 (28–30%), 3-(2-aminoethylamino) propyltrimethoxysilane (EDAS, $(CH_3O)_3Si(CH_2)_3NHCH_2CH_2NH_2$ (97%), potassium phosphate monobasic (KH_2PO_4), sodium chloride (NaCl), and potassium chloride (KCl) were purchased from Sigma-Aldrich; absolute ethanol (C_2H_5OH), hydrochloric acid (HCl (37%)), sodium hydroxide (NaOH), polyethylene glycol 400 Da (PEG 400), polyethylene glycol 10000 Da (PEG 10000), and polyethylene glycol 35000 Da (PEG 35000) from Merck; sodium phosphate dibasic (Na_2HPO_4) from Acros Organics; agarose from Eurogentec. Unless indicated otherwise, all these chemicals were ≥99% pure and were used without further purification. Phosphate Buffer Saline (PBS) solution was prepared using 1.4 mM KH_2PO_4, 10 mM Na_2HPO_4, 137 mM NaCl and 2.7 mM KCl and was adjusted at pH = 7.4 using 0.1 M HCl or 0.1 M NaOH.

2.2. Sample preparation

2.2.1. Silica gel synthesis

The synthesis is based on previous studies by our group [36,37]. Synthesis operating variables were selected in order to adopt a hydrolysis ratio (i.e. $[H_2O]/([TEOS] + 3/4\ [EDAS])$ equal to 5, a dilution ratio (i.e., $[C_2H_5OH]/([TEOS] + [EDAS])$) equal to 10, and a ratio of EDAS over TEOS (i.e. [EDAS]/[TEOS]) equal to 0.2. This gave a molar ratio TEOS: EDAS:ethanol:water:NH_3 of $1:0.2:24.08:5.75:1.84 \times 10^{-2}$.

The silica gel was synthesized in absolute ethanol, with TEOS, EDAS, and 0.18 M aqueous NH_3 solution. TEOS was first mixed with half of the ethanol under stirring. EDAS was then added under stirring. 0.18 M aqueous NH_3 solution and the other half of the ethanol were added to the mixture under vigorous stirring. The sample was then let for gelation and ageing in a closed vessel at 80 °C for 72 h. The silica gel was finally dried under air at room temperature for 72 h. After the synthesis, silica gels were grinded in a planetary mill (Pulverisette 6, Fritsch) for 10 cycles of 5 min at 500 rpm.

2.2.2. Hybrid agarose gel preparation

Agarose gels without silica (denoted AG) and with 2 wt% of silica (denoted AG-Si) were prepared. This proportion of silica was selected based on previous works studying the diffusion of large biomolecules in silica-agarose gels for different applications such as chromatography or separation [38,39].

The silica particles were dispersed in water in an ultrasonic bath for 6 h to obtain a 4 wt% silica dispersion. The dispersion was then kept in a water bath at 60 ℃ until mixing. In parallel, agarose was dissolved in water at 95 ℃ for 30 min to obtain a 2 wt% solution of agarose. The agarose solution was then kept in a water bath at 60 ℃ for 30 min before mixing. The final solution was prepared by adding the same volume of the silica dispersion and the agarose solution in a vial dipping in the water bath at 60 ℃. The vials were then mixed by inversion. 2.4 mL (degradation and thickness tests) or 500 µL (permeability test) of the final solution were placed in a petri dish of 3.5 cm in diameter (degradation and thickness tests) or in an insert of 12 mm in diameter (permeability test). The solution was then let to cool down at room temperature for 30 min. Agarose gels without silica were also prepared using the same procedure, but replacing the silica dispersion by water. The obtained gels were directly characterized to avoid dehydration.

2.3. Sample characterization

The organic content was determined by thermogravimetric analysis (TGA, TGA 7 from Perkin-Elmer) under air atmosphere at a heating rate of 20 ℃/min between 50 and 90 ℃ and 10 ℃/min between 90 and 750 ℃. The weight loss was measured between 150 and 750 ℃.

The textural properties were characterized by nitrogen adsorption-desorption isotherms in an ASAP 2420 multi-sampler adsorption-desorption volumetric device from Micromeritics. The surface area was evaluated using Brunauer, Emmett, and Teller theory (S_{BET}) [40,41]. V_P was defined as the specific liquid volume adsorbed at the saturation pressure of nitrogen. The mesoporous pore size distribution was determined by Barrett, Joyner, and Halenda theory [42,43].

The point of zero charge (PZC) was determined by the method of equilibrium pH at high loading [44]. The mass of the samples was first adjusted to obtain a surface loading equal to 10000 m^2/L in 20 mL (in line with previous studies [44,45]). The porous solids were then soaked for 3 h under stirring in 20 mL of water solutions of various starting pH ranging from 1 to 13 adjusted using HCl or NaOH solutions. After equilibration, the equilibrium pH was measured using an InLab Expert Pro-ISM electrode from Mettler Toledo. The PZC of the solid corresponds to a plateau in a plot of the final pH vs. the initial pH [44].

The silica gel particle size was investigated via scanning electron microscopy (SEM, ESEM XL30 from Philips) with accelerating voltage of 20 kV.

The hybrid agarose gel thickness was measured using a micrometer (Mitutoyo, 293-344) after equilibration at 25 ℃ for 1 h. The measurements were performed on three samples (5 times per replicate).

The dispersion of silica gel in the agarose gel were analyzed via SEM. The hybrid agarose gel samples were dehydrated in a graded ethanol series, then infiltrated successively in 1,2-propylene oxide, 1:1 propylene oxide/epoxy resin mix and then in pure epoxy resin. The samples were placed in silicon molds and left to polymerize at 60 ℃ for 72 h. The resin blocks were then polished and imaged at an accelerating voltage of 30 kV (energy dispersive X-ray analysis, EDX), 20 kV (secondary electron analysis, SE), 10 kV (back scattered electron analysis, BSE) with a scanning electron microscope (SEM, ESEM XL30 from Philips). The EDX analysis provides elemental identification and quantitative compositional information. The SE analysis shows the topography of the surface. The BSE analysis is used to detect contrast between areas with different chemical compositions (i.e. resin/agarose vs silica). The SE analysis was first performed on the sample to

detect the silica particles. The BSE and EDX analyses were then applied to confirm these observations.

The evolution of the macroscopic morphology of the hybrid agarose gels was followed by immersing the samples in 24 mL of PBS at 37 °C in closed vials. At scheduled times (i.e. 30 min, 4 h, 1 d, 1 week, 2 weeks, 4 weeks, 12 weeks), the samples were visually inspected and the pH of the supernatant was determined using an InLab Expert Pro-ISM electrode from Mettler Toledo. This analysis was performed in triplicates. As control, the evolution of the pH of a PBS solution was also followed.

The permeability of the hybrid agarose gels was assessed via a diffusion test. The inserts containing the gels were placed in wells of a 24-well cell culture plate containing 2.5 mL of mQ water. 500 µL of a 1 $mg \cdot mL^{-1}$ polyethylene glycol (PEG) solution containing PEG 400, 10000, and 35000 Da was placed on top of the gel. A schematic representation of the experimental set-up is presented in Figure S1. At scheduled times (i.e. 15 min, 30 min, 1 h, 4 h, 24 h), the solution in the well was removed, stored at −20 °C until analysis, and replaced by fresh mQ water. The PEG concentration was assessed via high performance liquid chromatography (HPLC) using PEG as standard. Chromatographic conditions were as follows: PL aquagel-OH mix 8 µm column (8 µm, 300 × 7.5 mm) followed by a PL aquagel-OH 308 µm column (8 µm, 300 × 7.5 mm), using milli-Q water as mobile phase at a flow rate of 1 $mL \cdot min^{-1}$ (pump: T1-series 1050 from Hewlett-Packard) at 30 °C (oven: CHM from Waters) with an evaporation light scattering detector with a gas flow rate of 1.3 $mL \cdot min^{-1}$ and a nebulization temperature of 40 °C (ELSD detector: 3300 ELSD from Alltech).

3. Results and discussion

3.1. Silica gel

As shown in the previous studies by our group, the proportion of ethylene diamine groups in the silica is equivalent to 22 wt%, which is close to the theoretical calculated value (i.e. 22.7 wt%) and corresponds to a concentration of 2.05 $mmol \cdot g^{-1}$ [36,37]. Regarding the texture, the specific surface area S_{BET} is equal to 330 $m^2 \cdot g^{-1}$ and the total pore volume V_P to 1.5 ± 0.1 $cm^3 \cdot g^{-1}$. The pore size distribution is characterized by the presence of a small peak at 8.8 nm and a larger peak at 18.7 nm. Finally, the point of zero charge (PZC) of the sample is 9.5. This means that the surface of the silica gel sample is positively charged at the pH of the morphology test (i.e. pH = 7.4), at agarose gel preparation (i.e. pH = 5), and at diffusion test (i.e. pH = 5).

The size and morphology of the silica particles is checked by SEM (Figure 1). Silica aggregates are present with a size ranging between 500–600 nm (encircled in red) and 10 µm (encircled in blue). These particles tend to agglomerate to form large structures with a size close to 50 µm.

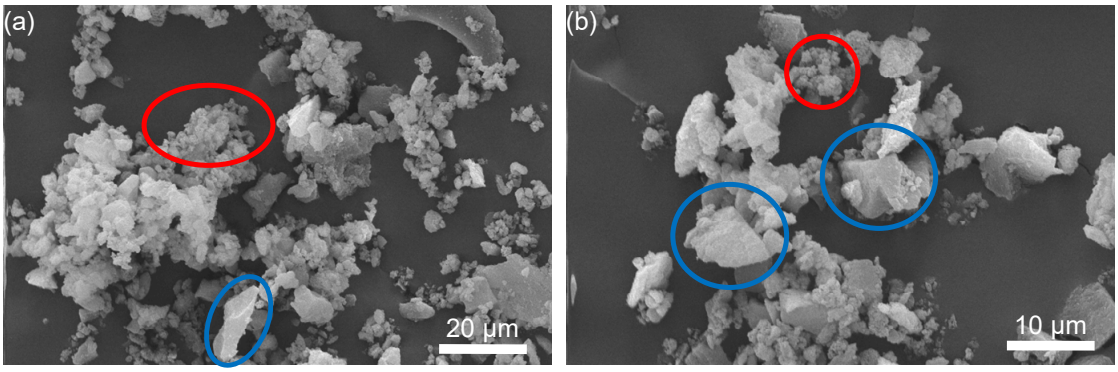

Figure 1. SEM images of the silica powder after grinding. Representative particle shapes are encircled: 500–600 µm in red and 10 µm in blue.

3.2. Hybrid agarose gels

Hybrid agarose is a valuable alternative to improve the osseointegration of synthetic substitutes for bone reconstruction. The possibility to incorporate and release active agents, such as proteins, makes this strategy even more attractive.

When dealing with thermally sensitive biomolecules like proteins, both the process and the materials have to be selected to prevent any denaturation, notably regarding temperature. For this reason, during hybrid gel preparation, the silica suspension and the agarose solution should be kept at 60 °C for a minimal duration, even though the encapsulation of the biomolecule inside the silica could protect it [46,47]. Furthermore, to guarantee the biomolecule stability, the melting and gelation temperature can be decreased by playing on the concentration of the agarose solution, the content in methoxy groups naturally present in agarose, or the pretreatment of the agarose (e.g. alkali treatment, methylation, hydroxyethylation) [48,49].

3.2.1. Physical aspect

According to our formulation procedure, the resulting gels discloses a flat surface. The agarose gels without silica (AG) are transparent while the agarose gel containing 2 wt% silica (AG-Si) are translucent (Figure 4, T0). It is worth to mention that the gelation rate is not affected by the presence of silica, all being formed within about 30 min.

The syneresis of hybrid silica-agarose gel is also compared to agarose gel by studying their thickness after equilibration at 25 °C for 1 h. The thickness of the AG sample was 2.1 ± 0.2 mm (mean ± standard deviation) and the one of the AG-Si sample was 1.9 ± 0.1 mm. No significant difference was observed, indicating that the presence of silica does not affect the equilibration equilibrium of agarose.

3.2.2. Microscopic morphology

The SEM images of the hybrid gel are presented in Figure 2a–d. Three kinds of analysis were performed. First, the topography was analyzed via the SE analysis. Then, the BSE analysis was applied to detect contrast between areas with different chemical compositions (i.e. resin/agarose vs

silica). Finally, the EDX analysis, which provides elemental identification and quantitative compositional information, was performed to detect the element present in each zone and determine if silica was present or not.

Contrary to the AG sample, which only exhibits a wave-like morphology, the AG-Si one presents agglomerates (indicated by a white arrow). As shown by the BSE analysis (Figure 2e–f), a difference in composition is observed between the agglomerates and the wave-like surface. This observation is confirmed by the EDX analysis (Figure 3). The agglomerates contain silicon, showing the presence of silica. On the opposite, the wave-like regions are only composed of carbon, oxygen, and chlorine, indicating the presence of agarose (i.e. carbon and oxygen) and resin (i.e. carbon, oxygen, and chlorine). Silica is therefore located in these aggregates.

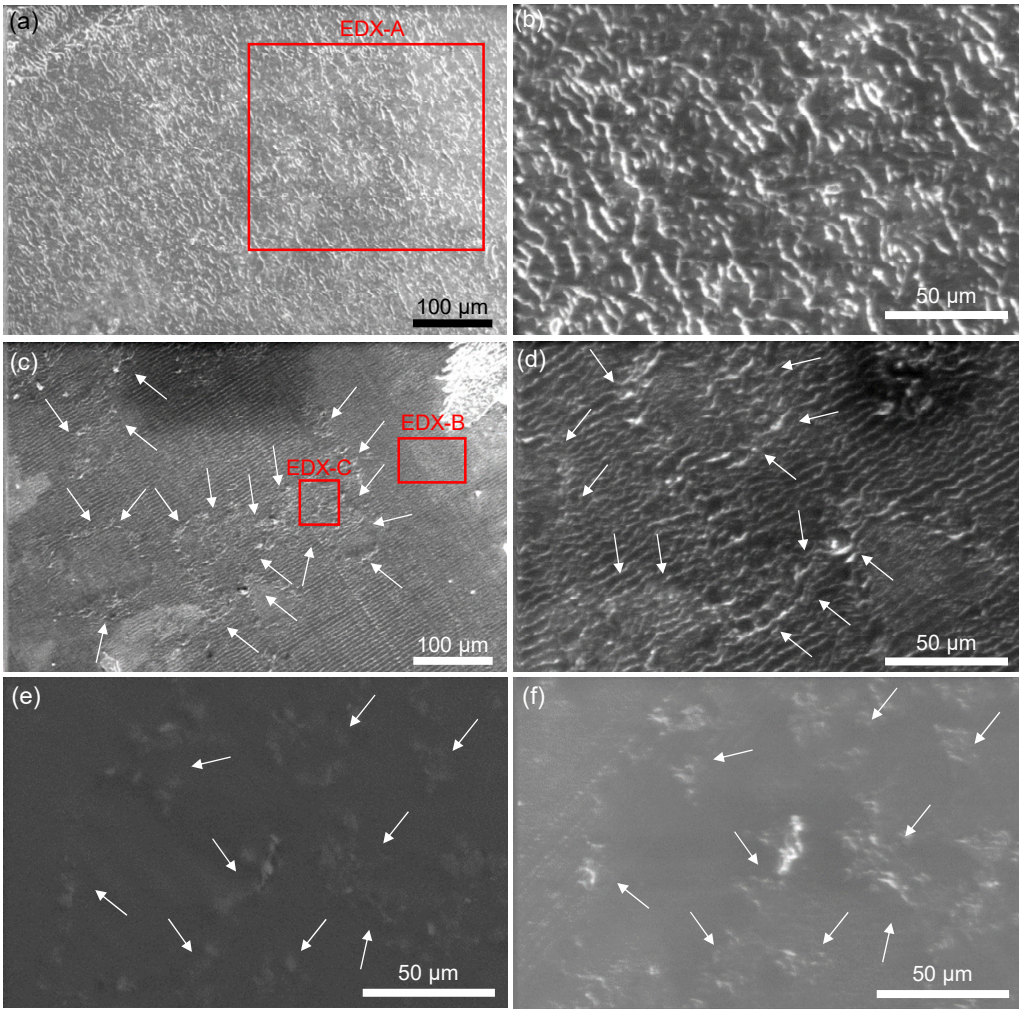

Figure 2. (a–d) SEM images of the (a–b) AG and (c–d) AG-Si samples using the SE detector. The red boxes correspond to the regions analyzed by EDX (Figure 3). (e,f) SEM images of the AG-Si sample using (e) the SE detector and (f) the BSE detector. Agglomerates are indicated by the white arrows.

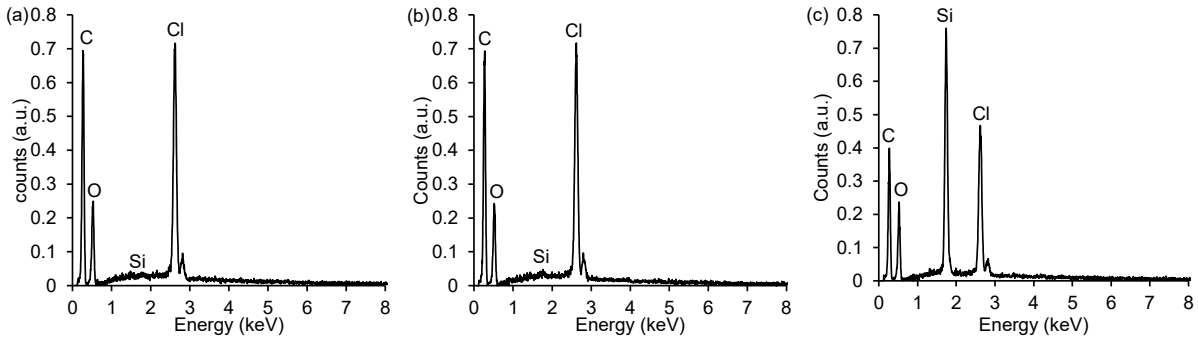

Figure 3. EDX analyses of (a) the wave-like region of the AG sample (i.e. EDX-A zone), (b) the wave-like region of the AG-Si sample (i.e. EDX-B zone), and (c) the aggregate region of the AG-Si sample (i.e. EDX-C zone). The EDX-n zone correspond to the red boxes of Figure 2.

The large size of these agglomerates (10–20 μm wide and over 100 μm long) is probably due to the presence of larger silica particles, as observed in the previous section (diameter close to 10 μm). These results show that silica is not finely dispersed in the materials but rather agglomerates randomly distributed in the agarose matrix.

Even not studied for agarose, it has been shown that the hydrophilicity of nanofillers directly affect the filler-matrix interactions and subsequently the filler dispersion [50]. In order to avoid the formation of aggregates, the hydrophilicity of the silica could therefore be increased by modifying its surface with a larger quantity of ethylene diamine groups. In this case, increasing the hydrophilicity of the silica would enhance the interactions between the silica and the agarose gel (mainly composed of water), which would decrease the presence of silica aggregates. However, a higher number of ethylene diamine groups may disturb the pH medium as discussed later on.

3.2.3. Evolution of the macroscopic morphology

The macroscopic morphology of the gels in PBS (pH = 7.4) is followed during 12 weeks (Figure 4). The visual inspection does not show any evolution in the macroscopic aspect of the gels up to 12 weeks. The samples present a flat and smooth surface over the 12 weeks. Moreover, no change in color or transparency is observed. Another interesting result is the absence of syneresis (i.e. shrinkage of the gel due to the expulsion of the solvent).

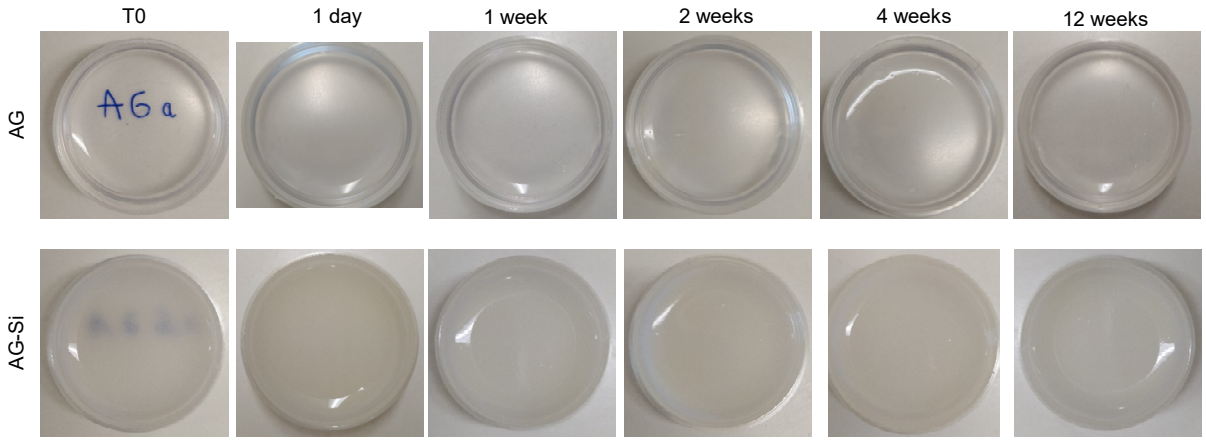

Figure 4. Evolution of the macroscopic morphology of the gels up to 12 weeks in PBS, pH = 7.4.

The pH of the supernatant is also followed over the 12-week period (Figure 5). For the AG sample, the pH remains constant over time, close to the value of the PBS. On the opposite, a pH increase of the supernatant is observed over the first 7 d of the test for the AG-Si sample. After day 7, the pH remains stable around 7.9. This slight alkalinisation of the buffer probably results from the basicity of the ethylene diamine groups grafted on the modified silica. As already observed in previous studies by our group, the pH of a silica dispersion in pure water tends to reach an equilibrium value, i.e. point of zero charge = 9.5 in milli-Q water at a surface loading of 10000 $m^2 \cdot L^{-1}$ [36,37]. In this case, due to the presence of a buffer and a lower surface loading (i.e. 700 $m^2 \cdot L^{-1}$), this value is not reached. Nevertheless, these results indicate that silica particles are well accessible to the surrounding water giving rise to the protonation of ethylene diamine groups.

Interestingly, this pH increase does not influence the macroscopic morphology of the hybrid gel. Nevertheless, this observation should be taken into account for future development, notably regarding cell cytotoxicity and adhesion.

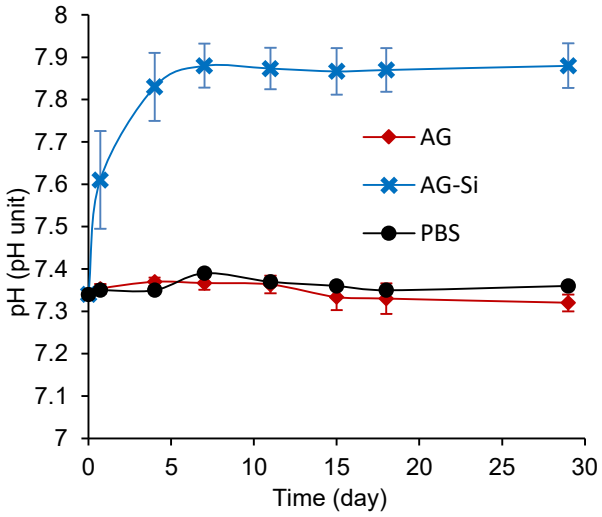

Figure 5. Evolution of the pH value of supernatant during the dissolution test.

3.2.4. Permeability test

The permeability study is an important assay to evaluate the diffusion ability of different proteins through the hydrogels. Being hydrosoluble and devoid from ionic charge, PEG is used as model biomarker to assess the permeability and porosity properties of agarose gels [51]. Available in a very wide range of molecular weight, it allows to easily assess the diffusion ability of macromolecules in function of their hydrodynamic radii. In practice, we have selected 3 PEG with Mn of 400, 10000, and 35000 Da, corresponding to hydrodynamic radii of 0.4–0.5 nm, 2.8–3.3 nm and 5.7–6.6 nm, respectively [52,53].

Their diffusion kinetics profiles over 24 h are depicted in Figure 6. No significant difference is observed between the AG and AG-Si samples, indicating that the addition of silica does not significantly influence the diffusion of the PEG molecules through the samples. On the opposite, the kinetics of diffusion is directly influenced by the molar weight of the PEG. Indeed, the PEG 400 is detected in the well after 1 h while 24 h are required for the PEG 10000 and 35000 to be detected. Moreover, after 24 h, 70–75% of PEG 400 diffuses through the agarose gels, while only 15–20% of PEG 10000 and 5–6% of PEG 35000 diffuses. This decrease in diffusion rate with molar weight can be assigned to the increase in hydrodynamic diameter and molar weight of PEG according to the Ogston model (Eq 1) [54]. This model hypothesizes that the diffusion of solutes in hydrogel involves a series of random unit steps, which stop when the solutes encounter the hydrogel fiber. The polymer gel is considered as a random network composed of long and straight fibers, while the diffusing solute is extrapolated as a hard sphere.

$$\frac{D_g}{D_0} = \exp\left[-\varphi^{0.5}\left(\frac{r_s + r_f}{r_f}\right)\right] \quad (1)$$

where D_g is the diffusion coefficient in the agarose gel ($m^2 \cdot s^{-1}$); D_0 is the diffusion coefficient at infinite diffusion (in the range of 2–3 × 10^{-10} $m^2 \cdot s^{-1}$ for agarose gels); φ is the volume fraction of polymer fibers in the hydrogel (in the range of 0.1–0.3 for agarose gels); r_f is the radius of the polymer fibers (1.9 × 10^{-9} m for agarose), and r_s is the radius of the solute (m). According to this model, increasing r_s, while keeping D_0, φ, and r_f constant, lead to a decrease in the diffusion coefficient in the agarose gel D_g.

This decrease in diffusion coefficient with increasing molar weights has already been observed for various polymers diffusing through agarose [33,55]. In the case of PEG, the evolution of the diffusion coefficient with the molar weight follows an exponential relation (Eq 2) [51].

$$D_g = 1.01 \times 10^{-8} \times MM^{-0.533} \quad (2)$$

where D_g is the diffusion coefficient in the agarose gel ($m^2 \cdot s^{-1}$) and MM is the molar weight of PEG (Da). The diffusion coefficients calculated from Eq 2 are equal to 4.1 × 10^{-10} $m^2 \cdot s^{-1}$ for PEG 400, 7.5 × 10^{-11} $m^2 \cdot s^{-1}$ for PEG 10000, and 3.8 × 10^{-11} $m^2 \cdot s^{-1}$ for PEG 35000.

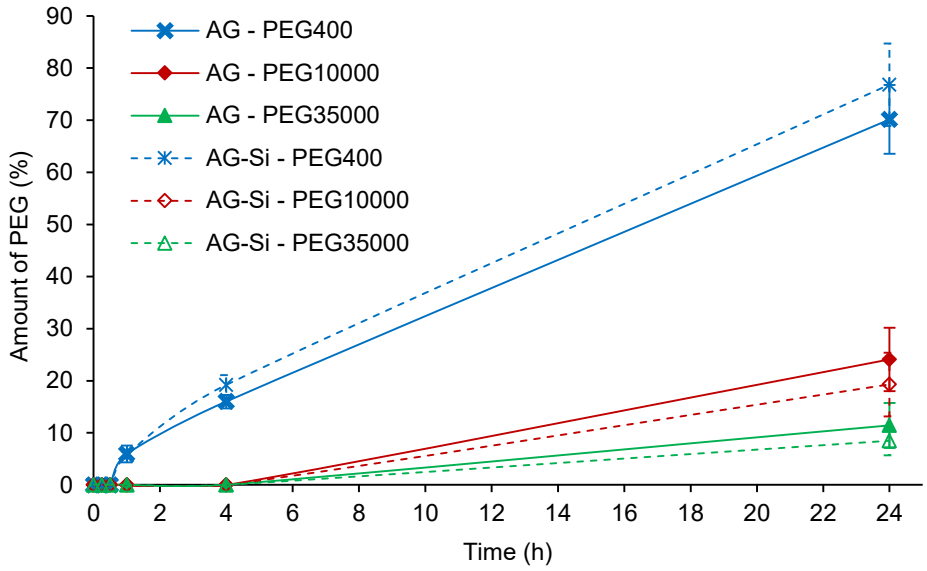

Figure 6. Diffusion kinetics profiles of PEG 400 (cross), PEG 10000 (diamond), and PEG 35000 (triangle) through the AG (full symbols and continuous lines) and AG-Si samples (empty symbols and dashed lines).

These results show that molecules larger than 3 nm can diffuse in 1-mm thick agarose gels in less than 24 h. As an example, if we consider an active protein to bone repair like the growth factor Bone Morphogenetic Protein-2 that exhibits a hydrodynamic diameter around 3–7 nm [36,37], it can be anticipated that the hybrid gel is not a barrier to its diffusion. Hybrid gel could therefore be used as a matrix to depose silica particles loaded with active macromolecules at the surface of scaffolds, for instance.

Nevertheless, this hypothetical analysis should be viewed cautiously, as PEG mainly interacts with agarose through frictional effects (i.e. solvent effects, steric hindrance), while proteins could also interact through attractive or repulsive forces [51,56].

4. Conclusions

In conclusion, this work suggests an alternative technique for the deposition of silica particles on the surface of bone substitute scaffolds. The strategy relies on the dispersion of silica particles in an agarose solution before proceeding to its deposition at the scaffold surface by gelation of the agarose matrix.

In this optic, ethylene diamine-modified silica with a wide size distribution, ranging between 500 nm and 10 µm, is added in agarose solutions in order to prepare a hybrid gel. Once added to the agarose, silica particles agglomerate in clusters (10-µm wide and over 100 µm-large) randomly distributed in the matrix.

Although preliminary, the present results have shown that hybrid agarose gel could represent an attractive matrix to disperse silica to bone substitute scaffolds. Indeed, the hybrid gels are stable over a 12-week period. Moreover, the silica particles are accessible to the surrounding medium. Finally, the presence of silica does not affect the diffusion kinetics of PEG through the hybrid gel. It is also

observed that PEG molecules larger than 3 nm could diffuse freely within 1 mm thick agarose gels in less than 24 h.

Nevertheless, an increase in pH of the supernatant was noticed for sample containing silica, which can be assigned to the ethylene diamine functional groups grafted on silica particles. This observation should be taken into account for the *in vitro* evaluation, as a change in pH of the cell culture medium could affect cell viability.

In further studies, the deposition of this material at the surface of the scaffold should also be investigated, notably via casting or dip-coating.

Acknowledgments

This work was supported by the Belgian Fund for Scientific Research (FNRS) under a Fund for Research Training in Industry and Agriculture (FRIA) grant, the "Ministère wallon de la Recherche et de l'Innovation", and the Walloon region. Julien G. Mahy and Ana P. F. Monteiro thank the F.R.S.-FNRS for their Postdoctoral Researcher position. Stéphanie D. Lambert thanks the F.R.S.-FNRS for her Senior Research Associate position. Rémi G. Tilkin and Nicolas Régibeau also thank the F.R.S.-FNRS for their FRIA grant.

The authors would like to thank Camille Tilkin.

Conflict of interest

The authors declare no conflict of interest.

References

1. Brydone AS, Meek D, MacLaine S (2010) Bone grafting, orthopaedic biomaterials, and the clinical need for bone engineering. *P I Mech Eng H* 224: 1329–1343. https://doi.org/10.1243/09544119JEIM770
2. Campana V, Milano G, Pagano E, et al. (2014) Bone substitutes in orthopaedic surgery: from basic science to clinical practice. *J Mater Sci-Mater M* 25: 2445–2461. https://doi.org/10.1007/s10856-014-5240-2
3. US Census Bureau (2012) Statistical abstracts of the United States: 2012-Section 1. Population. Available from: www.census.gov/library/publications/2011/compendia/statab/131ed/population.html.
4. Dimitriou R, Jones E, McGonagle D, et al. (2011) Bone regeneration: current concepts and future directions. *BMC Med* 9: 66. https://doi.org/10.1186/1741-7015-9-66
5. Wang M, Yang N (2017) A review of bioregulatory and coupled mechanobioregulatory mathematical models for secondary fracture healing. *Med Eng Phys* 48: 90–102. https://doi.org/10.1016/j.medengphy.2017.06.031
6. Baumhauer J, Pinzur MS, Donahue R, et al. (2014) Site selection and pain outcome after autologous bone graft harvest. *Foot Ankle Int* 35: 104–107. https://doi.org/10.1177/1071100713511434

7. Bolland BJRF, Wilson MJ, Howell JR, et al. (2017) An analysis of reported cases of fracture of the universal exeter femoral stem prosthesis. *J Arthroplasty* 32: 1318–1322. https://doi.org/10.1016/j.arth.2016.09.032
8. Othmani M, Aissa A, Bac CG, et al. (2013) Surface modification of calcium hydroxyapatite by grafting of etidronic acid. *Appl Surf Sci* 274: 151–157. https://doi.org/10.1016/j.apsusc.2013.03.002
9. Szubert M, Adamska K, Szybowicz M, et al. (2014) The increase of apatite layer formation by the poly(3-hydroxybutyrate) surface modification of hydroxyapatite and β-tricalcium phosphate. *Mater Sci Eng C-Mater* 34: 236–244. https://doi.org/10.1016/j.msec.2013.09.023
10. Tonon G, Morpurgo M (2006) Sol-gel derived silica polymers for the sustained release of proteins.
11. Chen YC, Liu CP, Yang CK, et al. (2013) Preparation and release properties of sol-gel encapsulated proteins. *JASMI* 3: 11–16. https://doi.org/10.4236/jasmi.2013.33A002
12. Zdarta J, Sałek K, Kołodziejczak-radzimska A, et al. (2015) Immobilization of Amano Lipase A onto Stöber silica surface: Process characterization and kinetic studies. *Open Chem* 13: 138–148. https://doi.org/10.1515/chem-2015-0017
13. Yang W, Hellner B, Baneyx F (2016) Self-immobilization of Car9 fusion proteins within high surface area silica sol-gels and dynamic control of protein release. *Bioconjug Chem* 27: 2450–2459. https://doi.org/10.1021/acs.bioconjchem.6b00406
14. Chen Y-C, Smith T, Hicks RH, et al. (2017) Thermal stability, storage and release of proteins with tailored fit in silica. *Sci Rep* 7: 46568. https://doi.org/10.1038/srep46568
15. Vlasenkova MI, Dolinina ES, Parfenyuk EV (2019) Preparation of mesoporous silica microparticles by sol-gel/emulsion route for protein release. *Pharm Dev Technol* 24: 243–252. https://doi.org/10.1080/10837450.2018.1457051
16. Andreani T, Souza ALRD, Silva AM, et al. (2012) Sol-gel carrier system: A novel controlled drug delivery, In: Souto EB, *Patenting Nanomedicines: Legal Aspects, Intellectual Property and Grant Opportunities*, Berlin, Heidelberg: Springer Berlin Heidelberg, 151–166. https://doi.org/10.1007/978-3-642-29265-1_5
17. Pirard SL, Mahy JG, Pirard JP, et al. (2015) Development by the sol-gel process of highly dispersed Ni-Cu/SiO_2 xerogel catalysts for selective 1,2-dichloroethane hydrodechlorination into ethylene. *Micropor Mesopor Mat* 209: 197–207. https://doi.org/10.1016/j.micromeso.2014.08.015
18. Wang X, Ahmed N Ben, Alvarez GS, et al. (2015) Sol-gel encapsulation of biomolecules and cells for medicinal applications. *Curr Top Med Chem* 15: 223–244. https://doi.org/10.2174/1568026614666141229112734
19. Reiner T, Kababya S, Gotman I (2008) Protein incorporation within Ti scaffold for bone ingrowth using sol-gel SiO_2 as a slow release carrier. *J Mater Sci-Mater M* 19: 583–589. https://doi.org/10.1007/s10856-007-3194-3
20. Ukmar T, Planinsek O (2010) Ordered mesoporous silicates as matrices for controlled release of drugs. *Acta Pharmceut* 60: 373–385. https://doi.org/10.2478/v1007-010-0037-4
21. Zhou Y, Quan G, Wu Q, et al. (2018) Mesoporous silica nanoparticles for drug and gene delivery. *Acta Pharm Sin B* 8: 165–177. https://doi.org/10.1016/j.apsb.2018.01.007

22. Kang S, Hong SI, Choe CR, et al. (2001) Preparation and characterization of epoxy composites filled with functionalized nanosilica particles obtained via sol-gel process. *Polymer* 42: 879–887. https://doi.org/10.1016/S0032-3861(00)00392-X
23. Bravo J, Zhai L, Wu Z, et al. (2007) Transparent superhydrophobic films based on silica nanoparticles. *Langmuir* 23: 7293–7298. https://doi.org/10.1021/la070159q
24. Elias L, Fenouillot F, Majesté JC, et al. (2008) Immiscible polymer blends stabilized with nano-silica particles: Rheology and effective interfacial tension. *Polymer* 49: 4378–4385. https://doi.org/10.1016/j.polymer.2008.07.018
25. Ghanbari A, Attar MM (2015) A study on the anticorrosion performance of epoxy nanocomposite coatings containing epoxy-silane treated nano-silica on mild steel substrate. *J Ind Eng Chem* 23: 145–153. https://doi.org/10.1016/j.jiec.2014.08.008
26. Jiang R, Kunz HR, Fenton JM (2006) Composite silica/Nafion ® membranes prepared by tetraethylorthosilicate sol-gel reaction and solution casting for direct methanol fuel cells. *J Membrane Sci* 272: 116–124. https://doi.org/10.1016/j.memsci.2005.07.026
27. Faustini M, Louis B, Albouy PA, et al. (2010) Preparation of sol-gel films by dip-coating in extreme conditions. *J Phys Chem C* 114: 7637–7645. https://doi.org/10.1021/jp9114755
28. Rocha CR, Chávez-Flores D, Zuverza-Mena N, et al. (2020) Surface organo-modification of hydroxyapatites to improve PLA/HA compatibility. *J Appl Polym* 137: 1–9. https://doi.org/10.1002/app.49293
29. Mano JF, Silva GA, Azevedo HS, et al. (2007) Natural origin biodegradable systems in tissue engineering and regenerative medicine: present status and some moving trends. *J R Soc Interface* 4: 999–1030. https://doi.org/10.1098/rsif.2007.0220
30. Buckley CT, Thorpe SD, Brien FJO, et al. (2009) The effect of concentration, thermal history and cell seeding density on the initial mechanical properties of agarose hydrogels. *J Mech Behav Biomed* 2: 512–521. https://doi.org/10.1016/j.jmbbm.2008.12.007
31. Miguel SP, Ribeiro MP, Brancal H, et al. (2014) Thermoresponsive chitosan-agarose hydrogel for skin regeneration. *Carbohyd Polym* 111: 366–373. https://doi.org/10.1016/j.carbpol.2014.04.093
32. Griess GA, Moreno ET, Herrmann R, et al. (1990) The sieving of rod-shaped viruses during agarose gel electrophoresis. I. comparison with the sieving of spheres. *Biopolymers* 29: 1277–1287. https://doi.org/10.1002/bip.360290816
33. Pluen A, Netti PA, Jain RK, et al. (1999) Diffusion of macromolecules in agarose gels : comparison of linear and globular configurations. *Biophys J* 77: 542–552. https://doi.org/10.1016/S0006-3495(99)76911-0
34. Paris JL, Lafuente-Gómez N, Cabañas MV, et al. (2019) Fabrication of a nanoparticle-containing 3D porous bone scaffold with proangiogenic and antibacterial properties. *Acta Biomater* 86: 441–449. https://doi.org/10.1016/j.actbio.2019.01.013
35. Kazimierczak P, Benko A, Palka K, et al. (2020) Novel synthesis method combining a foaming agent with freeze-drying to obtain hybrid highly macroporous bone scaffolds. *J Mater Sci Technol* 43: 52–63. https://doi.org/10.1016/j.jmst.2020.01.006
36. Tilkin RG, Colle X, Argento Finol A, et al. (2020) Protein encapsulation in functionalized sol-gel silica: Effect of the encapsulation method on the release kinetics and the activity. *Micropor Mesopor Mater* 308: 110502. https://doi.org/10.1016/j.micromeso.2020.110502

37. Tilkin RG, Mahy JG, Régibeau N, et al. (2021) Protein encapsulation in functionalized sol-gel silica: influence of organosilanes and main silica precursors. *J Mater Sci* 56: 14234–14256. https://doi.org/10.1007/s10853-021-06182-9
38. Rozaini MNH, Semail N-F, Saad B, et al. (2019) Molecularly imprinted silica gel incorporated with agarose polymer matrix as mixed matrix membrane for separation and preconcentration of sulfonamide antibiotics in water samples. *Talanta* 199: 522–531. https://doi.org/10.1016/j.talanta.2019.02.096
39. Pertoft H, Hallen A (1976) Preparation of silica-agarose beads for gel chromatography. *J Chromatogr A* 128: 125–131. https://doi.org/10.1016/S0021-9673(00)84038-8
40. Lecloux A (1971) Exploitation des isothermes d'adsorption et de désorption d'azote pour l'étude de la texture des solides poreux. *Mémoires Société des Sci Liege* 4: 169–209.
41. Lecloux A (1981) Texture of catalysts, In: Anderson JR, Boudart M, *Catalysis: Science and Technology*, Berlin, 171. https://doi.org/10.1007/978-3-642-93171-0_4
42. Pirard R, Heinrichs B, Cantfort OVAN, et al. (1998) Mercury porosimetry applied to low density xerogels; relation between structure and mechanical properties. *JSST* 13: 335–339. https://doi.org/10.1023/A:1008676211157
43. Lambert S, Alié C, Pirard JP, et al. (2004) Study of textural properties and nucleation phenomenon in Pd/SiO_2, Ag/SiO_2 and Cu/SiO_2 cogelled xerogel catalysts. *J Non Cryst Solids* 342: 70–81. https://doi.org/10.1016/j.jnoncrysol.2004.06.005
44. Park J, Regalbuto JR (1995) A simple, accurate determination of oxide PZC and the strong buffering effect of oxide surfaces at incipient wetness. *J Colloid Interface Sci* 175: 239–252. https://doi.org/10.1006/jcis.1995.1452
45. Lambert S, Job N, Souza LD, et al. (2009) Synthesis of very highly dispersed platinum catalysts supported on carbon xerogels by the strong electrostatic adsorption method. *J Catal* 261: 23–33. https://doi.org/10.1016/j.jcat.2008.10.014
46. Van Der Voort P, Esquivel D, et al. (2013) Periodic mesoporous organosilicas: from simple to complex bridges; a comprehensive overview of functions, morphologies and applications. *Chem Soc Rev* 42: 3913–3955. https://doi.org/10.1039/C2CS35222B
47. Manayil JC, Lee AF, Wilson K (2019) Functionalized periodic mesoporous organosilicas: tunable hydrophobic solid acids for biomass conversion. *Molecules* 24: 239. https://doi.org/10.3390/molecules24020239
48. te Nijenhuis K (1997) *Agarose, Thermoreversible Networks: Viscoelastic Properties and Structure of Gels*, Heidelberg, Springer Berlin Heidelberg, 194–202. https://doi.org/10.1007/BFb0008710
49. Lonza Appendix B: Agarose Physical Chemistry. Available from: http://www.lonzabio.jp/catalog/pdf/pd/PD029.pdf.
50. Régibeau N, Tilkin RG, Compère P, et al. (2020) Preparation of PDLLA based nanocomposites with modified silica by in situ polymerization: Study of molecular, morphological, and mechanical properties. *Mater Today Commun* 25: 101610. https://doi.org/10.1016/j.mtcomm.2020.101610
51. Weng L, Liang S, Zhang L, et al. (2005) Transport of glucose and poly(ethylene glycol)s in agarose gels studied by the refractive index method. *Macromolecules* 38: 5236–5242. https://doi.org/10.1021/ma047337w

52. Devanand K, Selser JC (1991) Asymptotic behavior and long-range interactions in aqueous solutions of poly(ethylene oxide). *Macromolecules* 24: 5943–5947. https://doi.org/10.1021/ma00022a008
53. Fee CJ, Van Alstine JM (2004) Prediction of the viscosity radius and the size exclusion chromatography behavior of PEGylated proteins. *Bioconjug Chem* 15: 1304–1313. https://doi.org/10.1021/bc049843w
54. Ogston AG, Preston BN, Wells JD (1973) On the transport of compact particles through solutions of chain-polymers. *Proc R Soc A* 333: 297–316. https://doi.org/10.1098/rspa.1973.0064
55. Karlsson D, Zacchi G, Axelsson A (2002) Electronic speckle pattern interferometry: A tool for determining diffusion and partition coefficients for proteins in gels. *Biotechnol Prog* 18: 1423–1430. https://doi.org/10.1021/bp0255659
56. Monteiro APF, Idczak G, Tilkin RG, et al. (2021) Evaluation of hydroxyapatite texture using CTAB template and effects on protein adsorption. *Surf Interfaces* 27: 101565. https://doi.org/10.1016/j.surfin.2021.101565

AIMS Press